Supporting Information
for

Integration of Simultaneous and Cascade Release of Two Drugs from Smart Single Nanovehicles Based on DNA-Gated Mesoporous Silica Nanoparticles

Shengwang Zhou, Huizi Sha, Baorui Liu and Xuezhong Du*

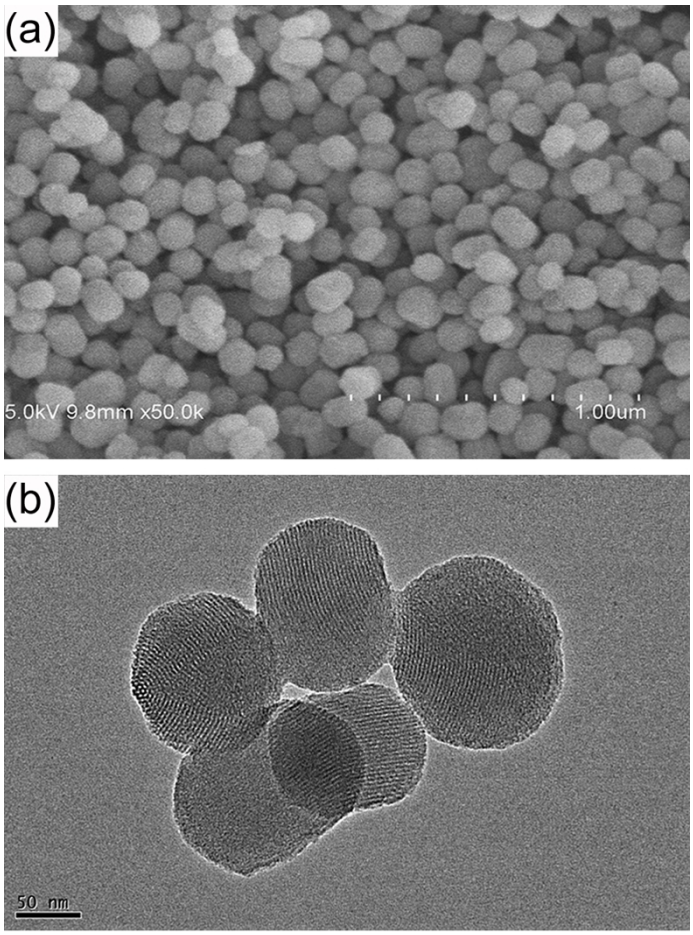

Fig. S1 SEM (a) and TEM (b) images of MCM-41 nanoparticles.

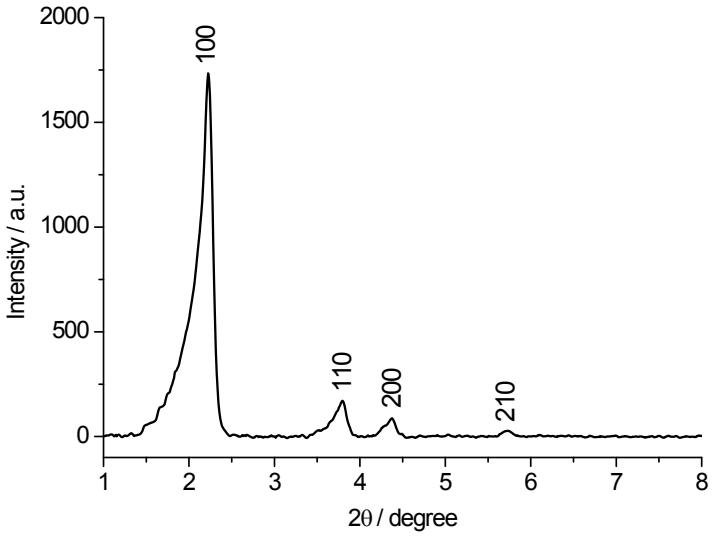

Fig. S2 Small-angle powder XRD patterns of MCM-41 nanoparticles.

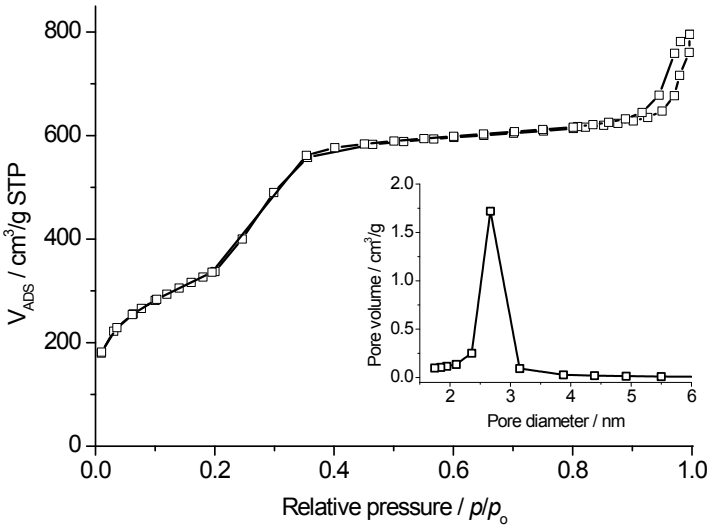

Fig. S3 Nitrogen adsorption–desorption isotherms of MCM-41 nanoparticles. Inset shows pore size distribution.

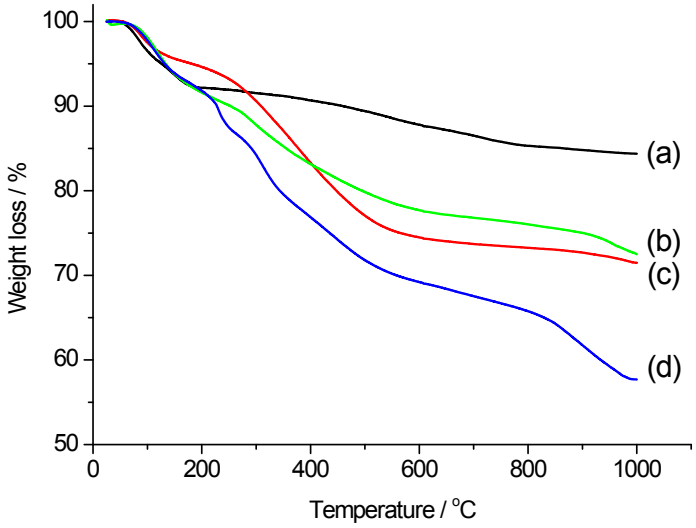

Fig. S4 Thermogravimetric analysis profiles of (a) MCM-41, (b) phosphonate-functionalized MSNs (MSN-POH), (c) Ti^{IV}-chelating phosphonate-functionalized MSNs (MSN-PO-Ti), (d) spDNA-gated MSNs without cargo loading (MSN-PO-Ti-DNA).

The surface density of the phosphonate functionalities on the MSN surfaces was determined to be 0.6714 mmol/g MSN by thermogravimetric analysis. At elevated temperatures up to 1000 °C, both adsorbed species and modified organic functionalities on the MSN surfaces were completely removed and decomposed. The weight loss of MCM-41 (bare MSNs, curve a) was used as a reference for adsorbed species. The difference of weight loss between the phosphonate-functionalized MSNs (MSN-POH, curve b) and MCM-41 (curve a) was used to calculate the surface density of the phosphonate functionalities on the MSN surfaces considering the molecular weight of the phosphonate functionalities. Similarly, the difference of weight loss between the spDNA-gated Ti^{IV}-chelating phosphonate-functionalized MSNs (MSN-PO-Ti-DNA, curve d) and Ti^{IV}-chelating phosphonate-functionalized MSNs (MSN-PO-Ti, curve c) was used to calculate the capping amount of spDNA for the phosphonate-functionalized MSNs.

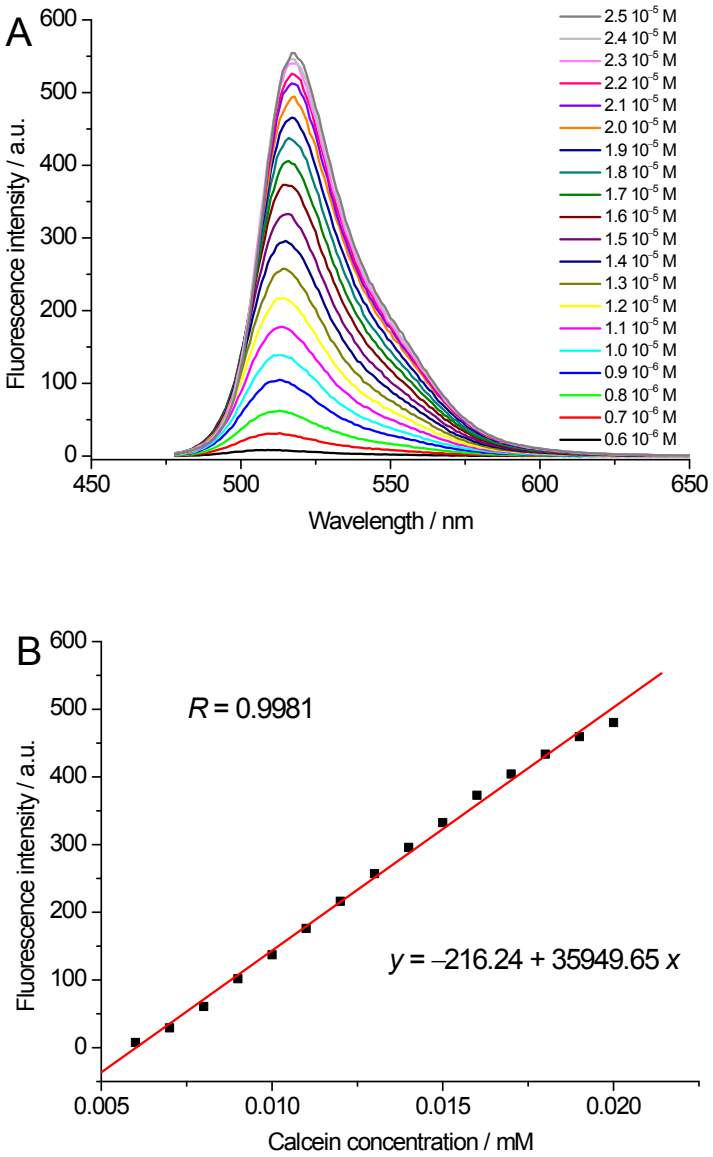

Fig. S5 (A) Fluorescence spectra of aqueous calcein in PBS solutions (pH 7.4) with different concentrations at the excitation wavelength of 458 nm. (B) Fluorescence intensity at 510 nm as a function of calcein concentration. (C) Fluorescence spectrum of final washing solution containing unloaded calcein in 250 mL of PBS solution at the excitation wavelength of 458 nm.

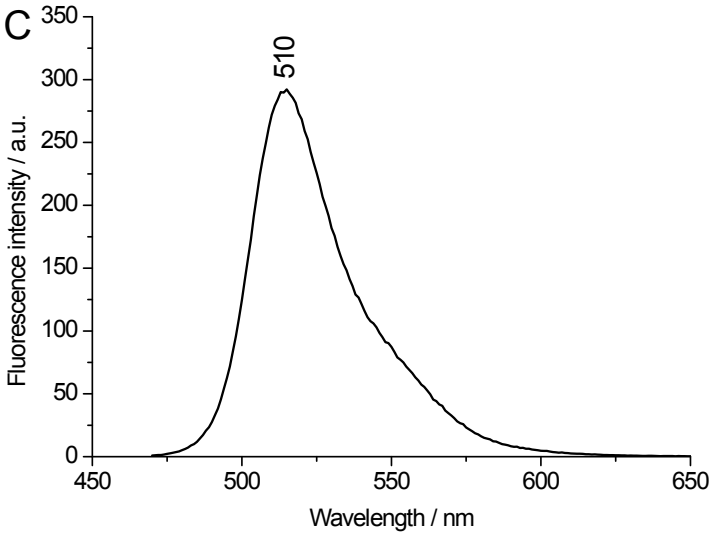

Fig. S5 (continuted)

The loading of calcein was carried out as follows. First, 20 mg of Ti^{4+}-chelating phosphonate-functionalized MSNs (MSN-PO-Ti) were suspended in 10 mL of aqueous calcein (0.4 mM) in PBS solution for calcein loading. Second, aqueous spDNA solution was added to the suspension for DNA capping. Third, 5 mL of aqueous 9-aminoacridine solution (1 mM) was added for 9-aminoacridine loading, followed by centrifugation and washing with PBS solution to remove excess cargo and DNA. Finally, the washing solutions were collected and diluted to a certain volume of 250 mL. The fluorescence spectrum of the final washing solution was measured (Fig. S5C), and the concentration of the final washing solution was determined from the standard curve of fluorescence intensity of aqueous calcein solution versus concentration (Fig. S5A,B). The difference between the initially added (total) and unloaded (washed) amounts of calcein was calculated to determine the loading capacity of calcein encapsulated within the Ti^{4+}-chelating phosphonate-functionalized MSNs.

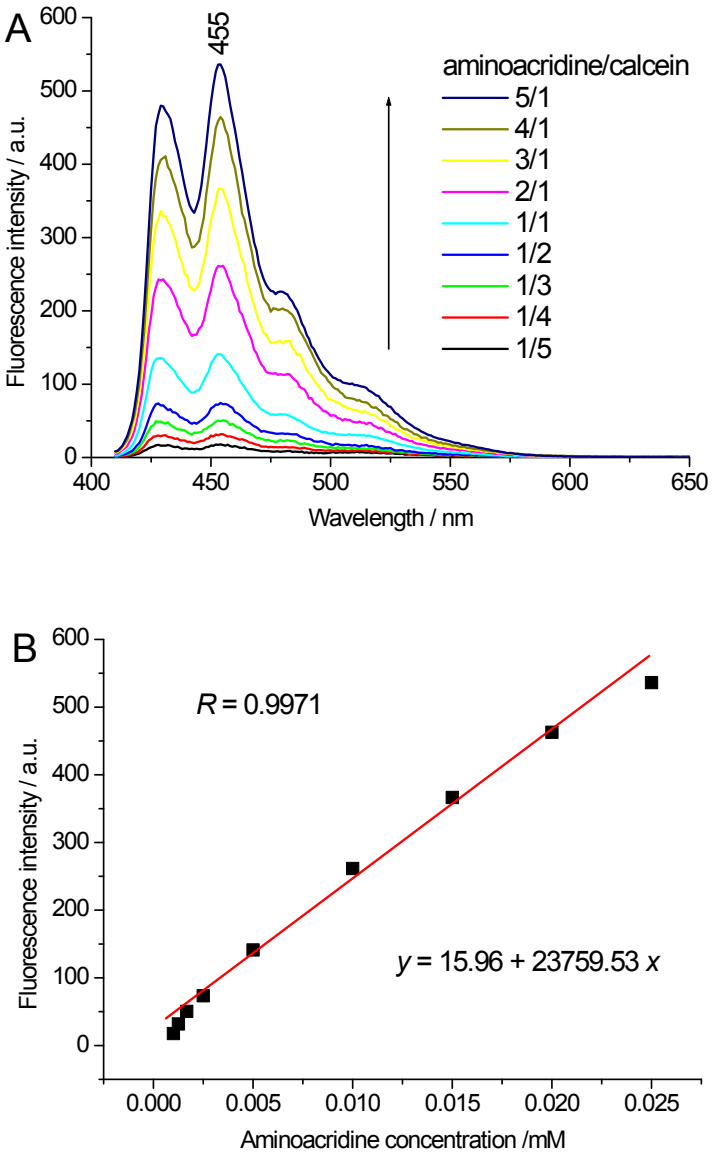

Fig. S6 (A) Fluorescence spectra of the solution mixtures of 9-aminoacridine and calcein with different molar ratios (λ_{ex} = 400 nm) when the calcein concentration was fixed at 0.005 mM. (B) Fluorescence intensity at 455 nm as a function of concentration of 9-aminoacridine in the solution mixtures. (C) Fluorescence spectrum of final washing solution containing unloaded 9-aminoacridine and calcein in 250 mL of PBS solution at the excitation wavelength of 400 nm.

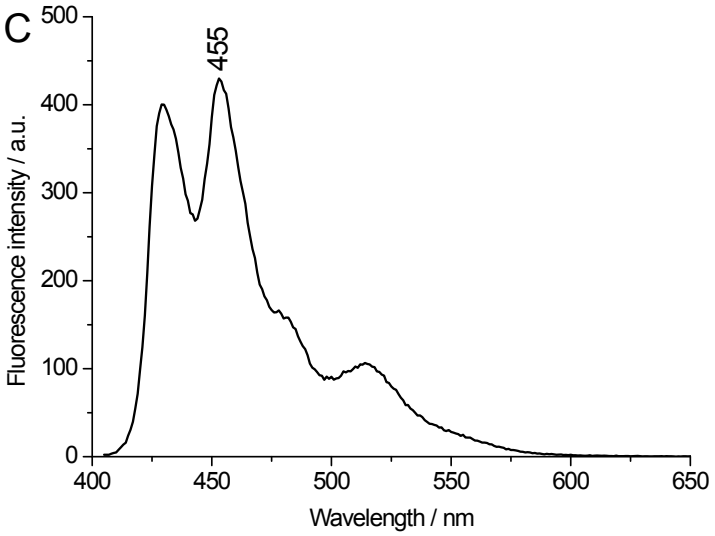

Fig. S6 (continuted)

The loading of 9-aminoacridine was carried out as follows. First, 20 mg of Ti^{IV}-chelating phosphonate-functionalized MSNs (MSN-PO-Ti) were suspended in 10 mL of aqueous calcein (0.4 mM) in PBS solution for calcein loading. Second, aqueous spDNA solution was added to the suspension for DNA capping. Third, 5 mL of aqueous 9-aminoacridine solution (1 mM) was added for 9-aminoacridine loading, followed by centrifugation and washing with PBS solution to remove excess cargo and DNA. Finally, the washing solutions were collected and diluted to a certain volume of 250 mL. The fluorescence spectrum of the final washing solution was measured (Fig. S6C), and the concentration of the final washing solution was determined from the standard curve of fluorescence intensity of the solution mixtures of 9-aminoacridine and calcein with different molar ratios (λ_{ex} = 400 nm) versus 9-aminoacridine concentration (Fig. S6A,B). The difference between the initially added (total) and unloaded (washed) amounts of 9-aminoacridine was calculated to determine the loading capacity of 9-aminoacridine intercalating within the capped spDNA.

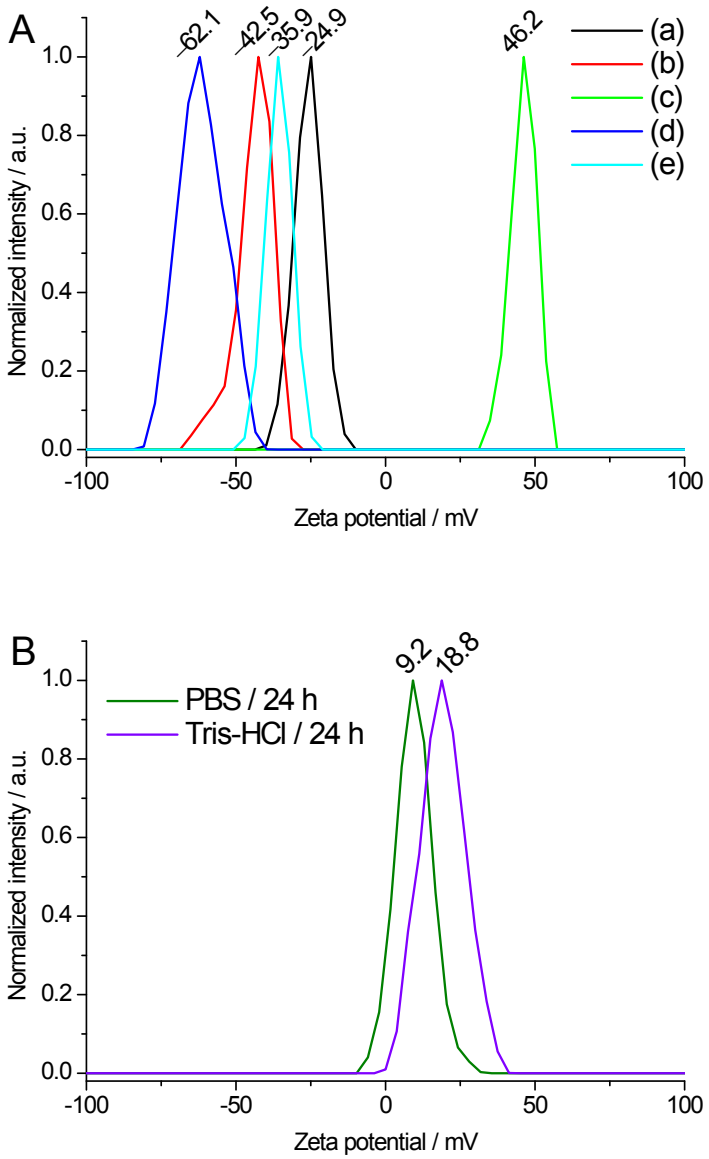

Fig. S7 (A) Zeta potentials of (a) MCM-41, (b) phosphonate-functionalized MSNs (MSN-POH), (c) Ti^{IV}-chelating phosphonate-functionalized MSNs (MSN-PO-Ti), (d) spDNA-gated MSNs without cargo loading (MSN-PO-Ti-DNA), and (e) spDNA-gated MSNs with the intercalation of 9-aminoacridine in PBS solution (pH 7.4). (B) Zeta potentials of Ti^{IV}-chelating phosphonate-functionalized MSNs (MSN-PO-Ti) in PBS solution (pH 7.4) and Tris-HCl buffer (pH 7.4) after 24 h of stirring.

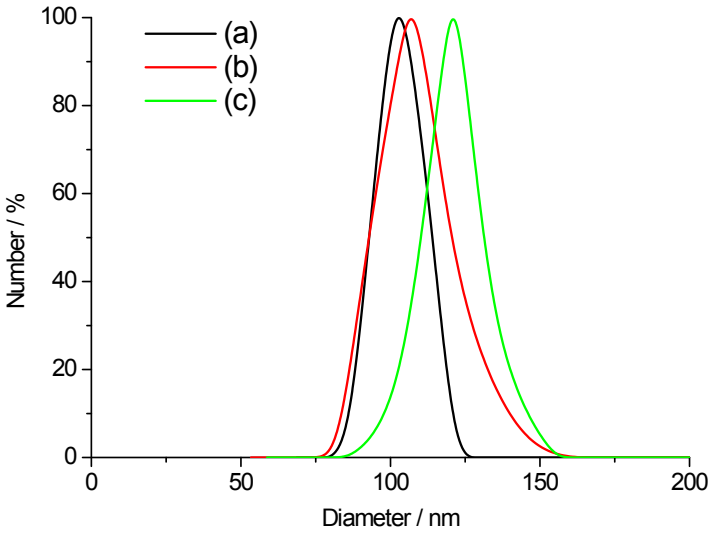

Fig. S8 Hydrodynamic diameter distributions of (a) MCM-41, (b) Ti^{IV}-chelating phosphonate-functionalized MSNs (MSN-PO-Ti), and (c) spDNA-gated MSNs without cargo loading (MSN-PO-Ti-DNA) in PBS solution (pH 7.4).

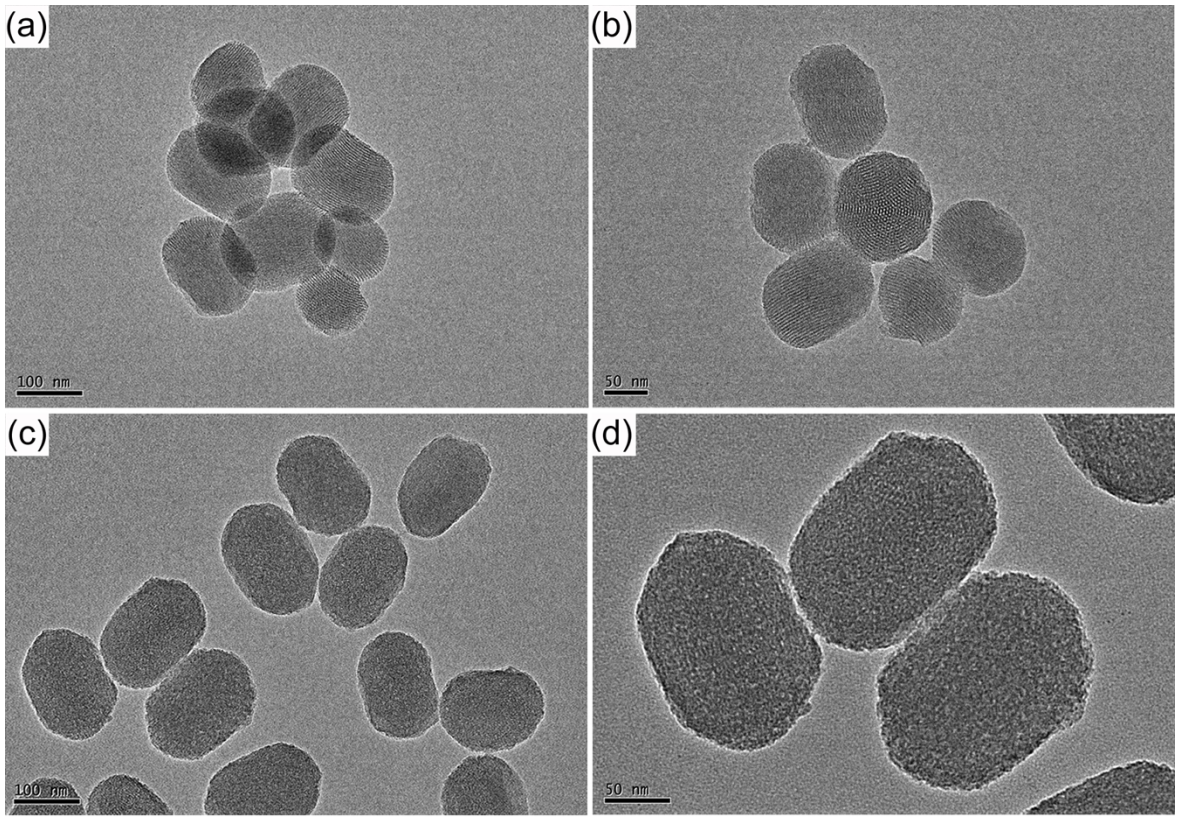

Fig. S9 TEM images in different scales of (a,b) Ti^{IV}-chelating phosphonate-functionalized MSNs (MSN-PO-Ti) and (c,d) spDNA-gated MSNs without cargo loading (MSN-PO-Ti-DNA).

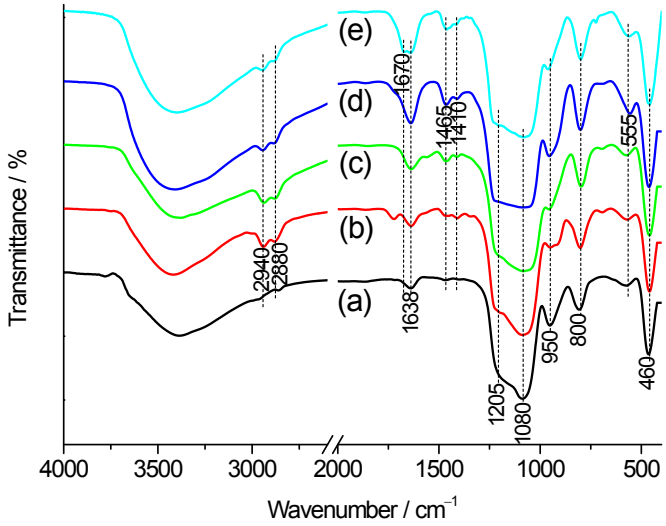

Fig. S10 FTIR spectra of (a) MCM-41, (b) glycidoxypropyl-functionalized MSNs, (c) ethylenediamine-functionalized MSNs, (d) phosphonate-functionalized MSNs (MSN-POH), and (e) Ti^{IV}-chelating phosphonate-functionalized MSNs (MSN-PO-Ti).

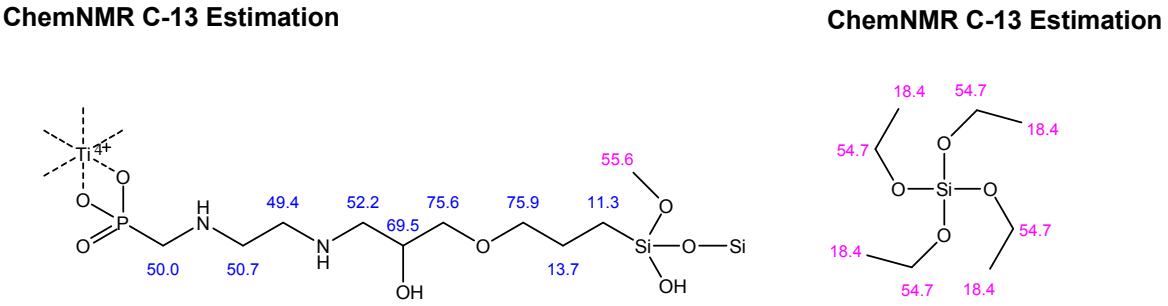

The resonances around 23 ppm most likely resulted from not fully condensed MSNs.

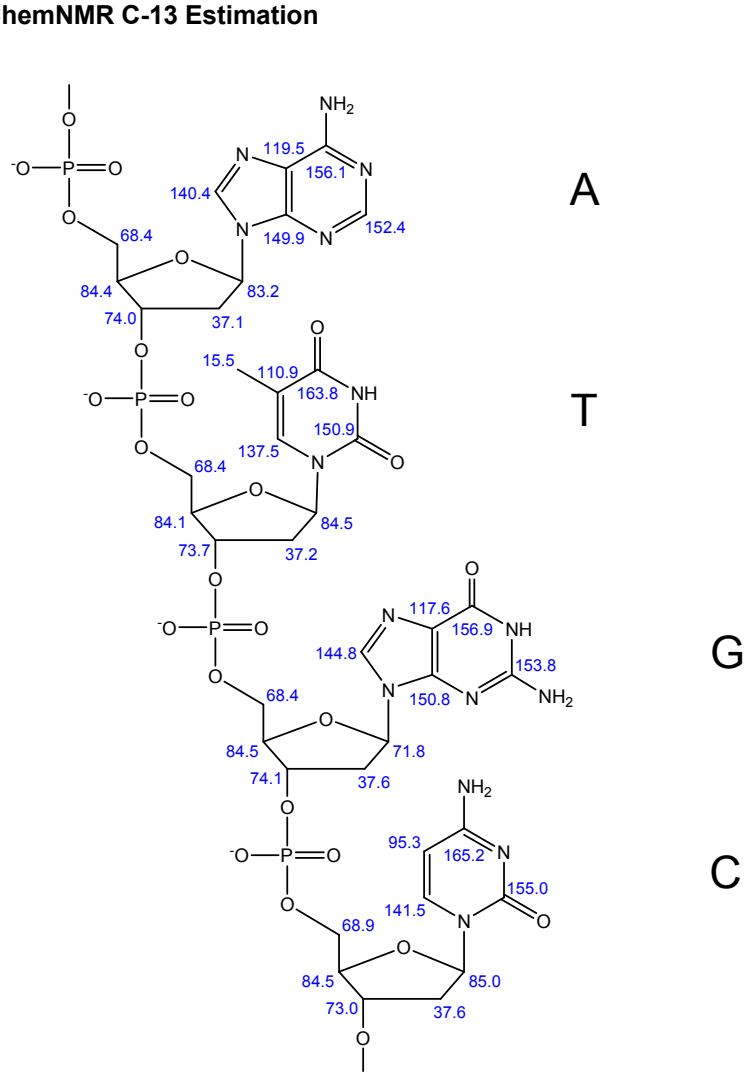

Fig. S11 Assignments of ^{13}C NMR spectra (ppm) of (a) Ti^{IV}-chelating phosphonate-functionalized MSNs (MSN-PO-Ti) and (b) DNA fragments.

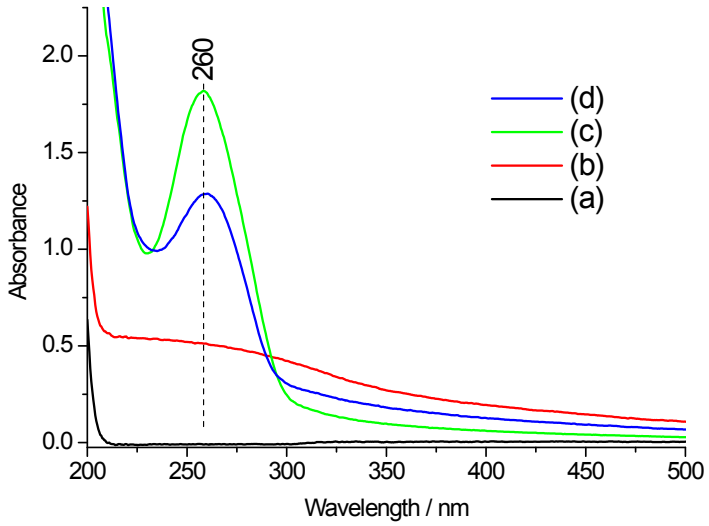

Fig. S12 UV-vis spectra of (a) PBS solution, (b) Ti^{IV}-chelating phosphonate-functionalized MSNs (MSN-PO-Ti) in PBS solution (1 mg/mL), (c) spDNA in PBS solution (0.2 mg/mL), and (d) spDNA-gated MSNs without cargo loading (MSN-PO-Ti-DNA) in PBS solution (1 mg/mL).

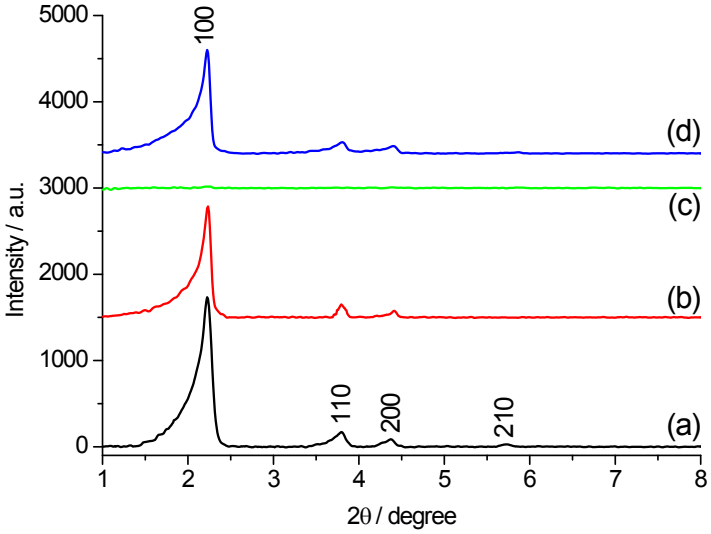

Fig. S13 Small-angle powder XRD patterns of (a) MCM-41, (b) Ti^{IV}-chelating phosphonate-functionalized MSNs (MSN-PO-Ti), and spDNA-gated MSNs with the loading of calcein and 9-aminoacridine (c) before and (d) after cargo release upon trigger of DNase I (20 U/mL).

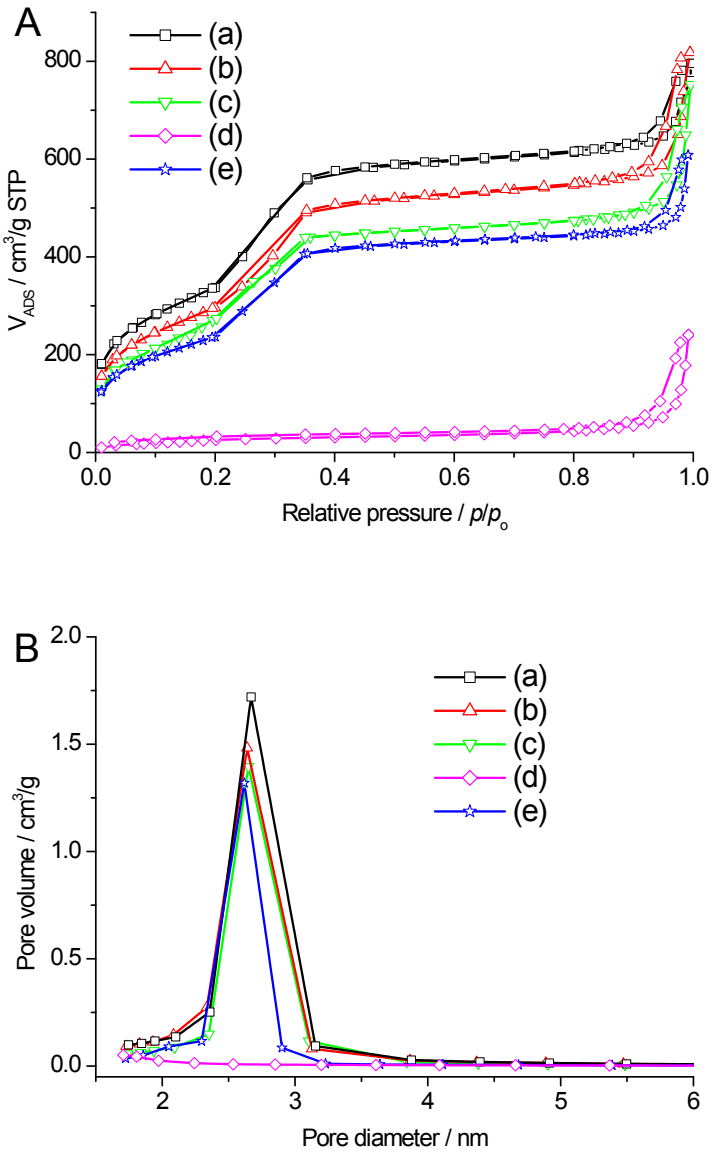

Fig. S14 (A) Nitrogen adsorption–desorption isotherms and (B) pore size distributions of (a) MCM-41, (b) phosphonate-functionalized MSNs (MSN-POH), (c) Ti^{IV}-chelating phosphonate-functionalized MSNs (MSN-PO-Ti), and spDNA-gated MSNs with the loading of calcein and 9-aminoacridine (d) before and (e) after cargo release upon trigger of DNase I (20 U/mL).

Table S1. Surface areas and average pore sizes of MSN materials calculated from the nitrogen adsorption–desorption isotherms.

materials	surface area (m^2/g)	pore size (nm)
MCM-41	1174.6	2.67
phosphonate-functionalized MSNs	1030.3	2.64
Ti^{IV}-chelating phosphonate-functionalized MSNs	865.8	2.65
calcein and 9-aminoacridine-loaded, spDNA-gated MSNs	49.2	–
spDNA-gated MSNs after cargo release triggered by DNase I	821.8	2.62

Surface areas, cumulative pore volumes, and pore size distributions of a variety of MSN materials were determined from nitrogen adsorption–desorption isotherms (Brunauer-Emmett-Teller (BET) adsorption) on a Micromeritics ASAP2020 porosimeter at 77 K. These data were directly obtained from automatic data output of the instrument. The average pore sizes (Barrett-Joyner-Halenda (BJH) pore size distribution) were easily obtained from the plots of cumulative pore volume as a function of pore size. The methods and detailed explanation were described in the literature.[S1,S2]

References

S1 S. Brunauer, P. H. Emmett and E. Teller, *J. Am. Chem. Soc.*, 1938, **60**, 309–319.
S2 E. P. Barrett, L. G. Joyner and P. P. Halenda, *J. Am. Chem. Soc.*, 1951, **73**, 373–380.

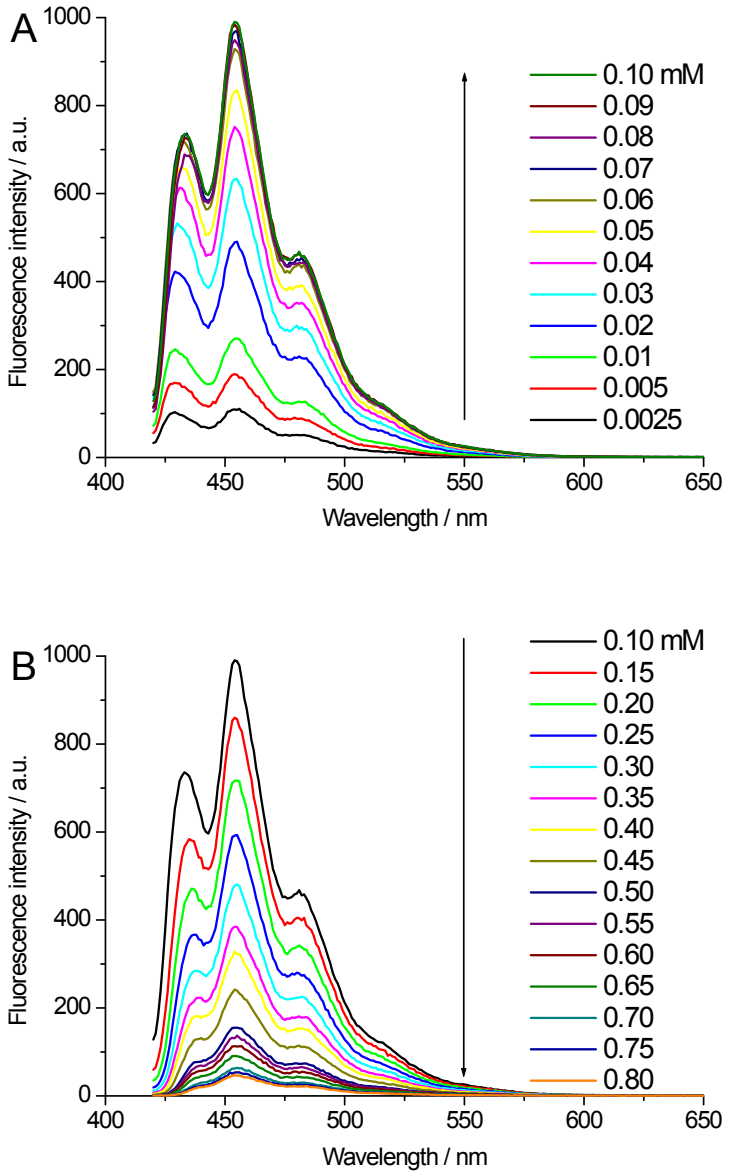

Fig. S15 Fluorescence spectra of aqueous 9-aminoacridine solutions with different concentrations at the excitation wavelength of 400 nm.

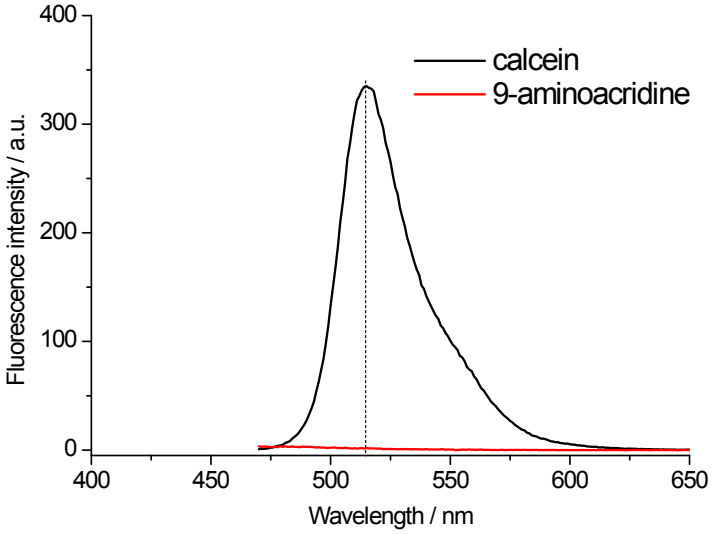

Fig. S16 Comparison of fluorescence spectra of calcein and 9-aminoacridine (0.015 mM) at the excitation wavelength of 458 nm.

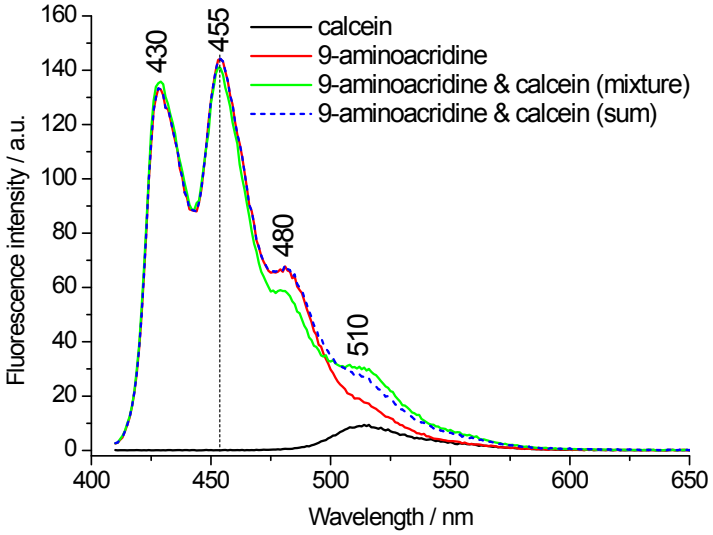

Fig. S17 Comparison of fluorescence spectra of 9-aminoacridine and calcein with equimolar mixture (calcein concentration at 0.005 mM) and their sum at the excitation wavelength of 400 nm.

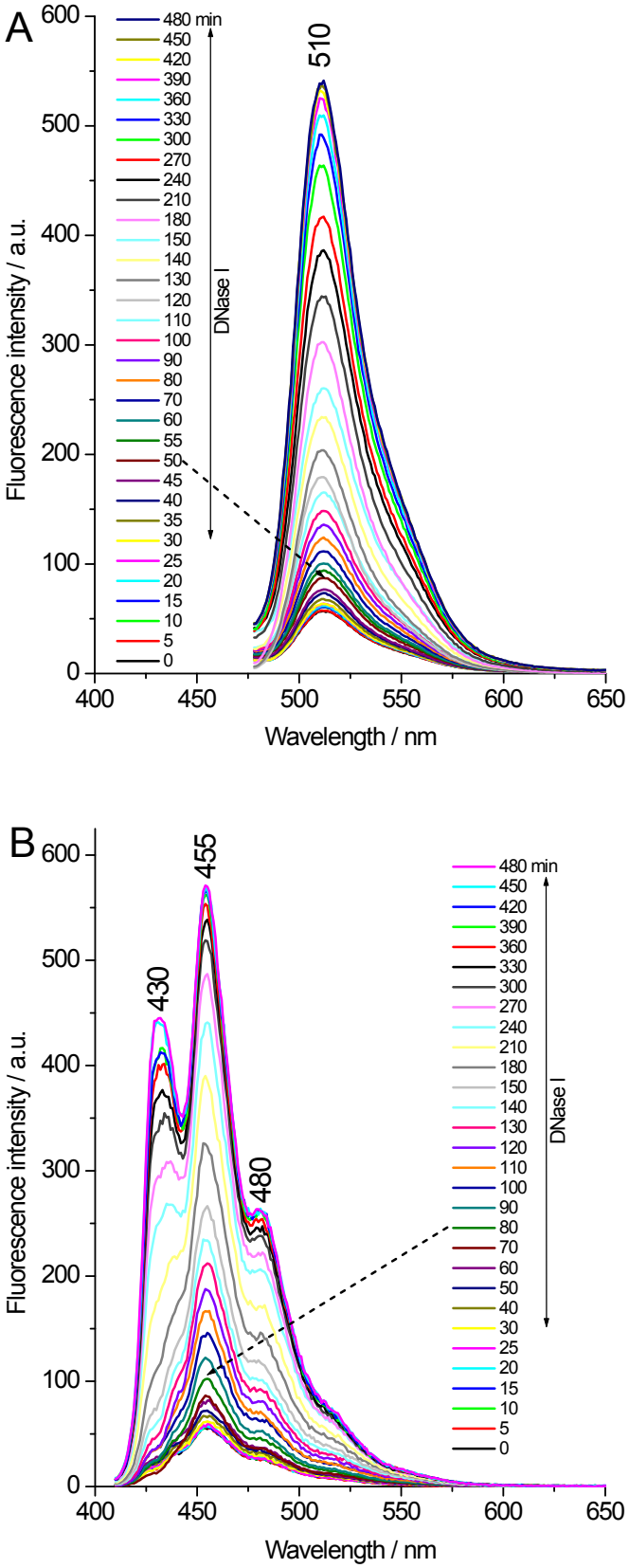

Fig. S18 Fluorescence spectra of dyes released from the PBS solution (pH 7.4) of spDNA-gated MSNs functionalized with Ti^{IV}-chelating phosphonates (MSN-PO-Ti-DNA) upon addition of DNase I (20 U/mL) after 30 min: (A) calcein (λ_{ex} = 458 nm, λ_{em} = 510 nm); (B) 9-aminoacridine (λ_{ex} = 400 nm, λ_{em} = 455 nm).

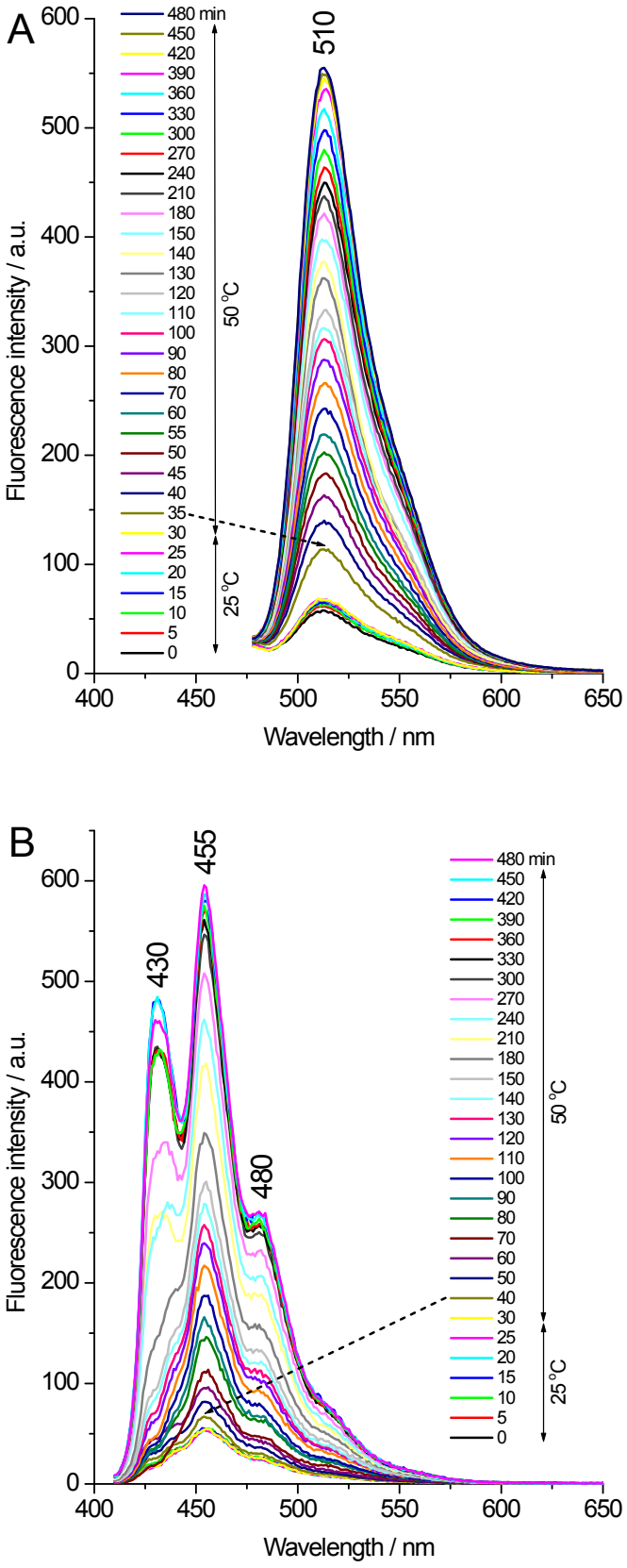

Fig. S19 Fluorescence spectra of dyes released from the PBS solution (pH 7.4) of spDNA-gated MSNs functionalized with Ti^{IV}-chelating phosphonates (MSN-PO-Ti-DNA) upon change of temperature from 25 °C to 50 °C after 30 min: (A) calcein (λ_{ex} = 458 nm, λ_{em} = 510 nm); (B) 9-aminoacridine (λ_{ex} = 400 nm, λ_{em} = 455 nm).

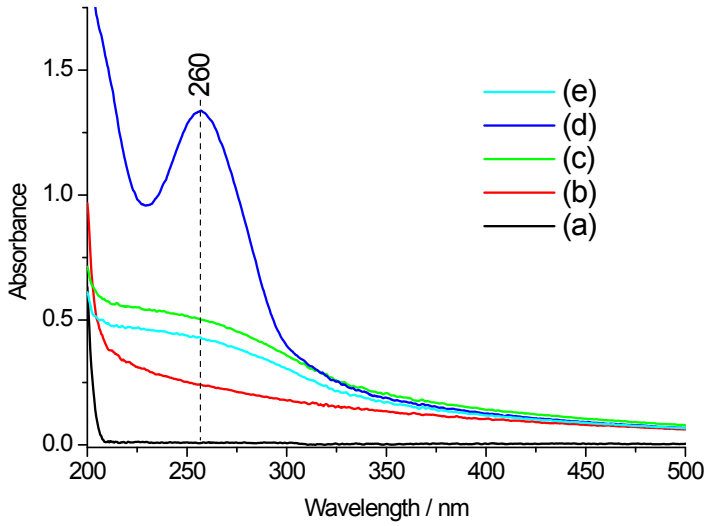

Fig. S20 UV-vis spectra of (a) Tris-HCl buffer (pH 7.4), (b) phosphonate-functionalized MSNs (MSN-POH) in Tris-HCl buffer (1 mg/mL), (c) Ti^{IV}-chelating phosphonate-functionalized MSNs (MSN-PO-Ti) in Tris-HCl buffer (1 mg/mL), and spDNA-gated MSNs without cargo loading (MSN-PO-Ti-DNA) in Tris-HCl buffer (1 mg/mL) (d) before and (e) after heating of 50 °C for 8 h followed centrifugation.

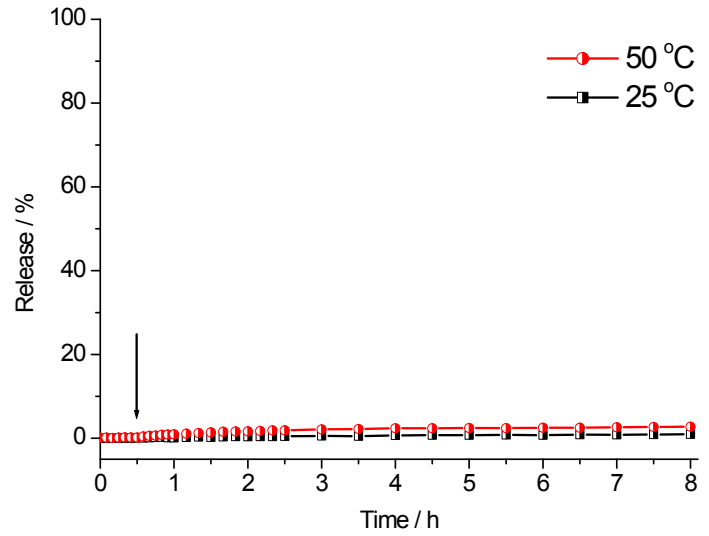

Fig. S21 Comparison of release profiles from the phosphonate-functionalized MSNs (MSN-POH) in the absence of Ti^{IV} after addition of calcein and spDNA (followed by washing) upon change of temperature from 25 °C to 50 °C after 30 min in PBS solutions (pH 7.4): calcein (λ_{ex} = 458 nm, λ_{em} = 510 nm). The arrow indicates the change of temperature.

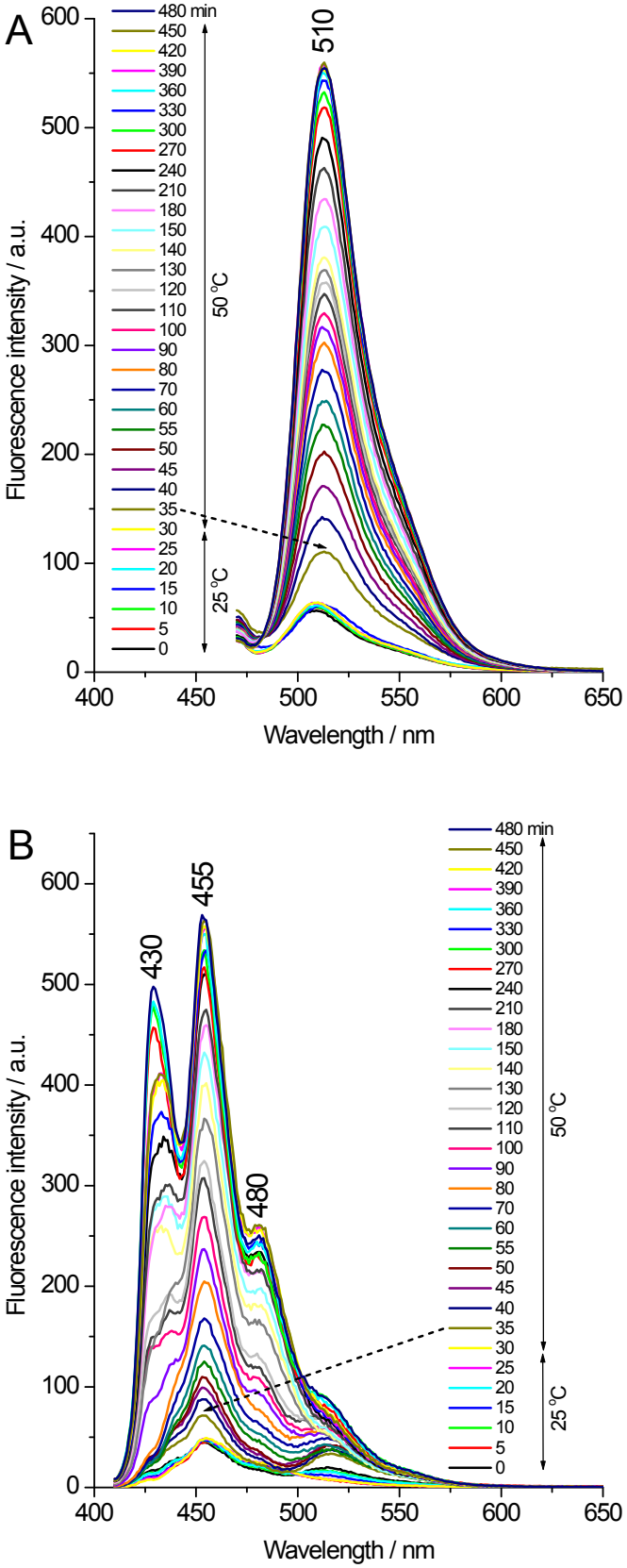

Fig. S22 Fluorescence spectra of dyes released from the Tris-HCl buffer (pH7.4) of spDNA-gated MSNs functionalized with Ti^{IV}-chelating phosphonates (MSN-PO-Ti-DNA) upon change of temperature from 25 °C to 50 °C after 30 min: (A) calcein (λ_{ex} = 458 nm, λ_{em} = 510 nm); (B) 9-aminoacridine (λ_{ex} = 400 nm, λ_{em} = 455 nm).

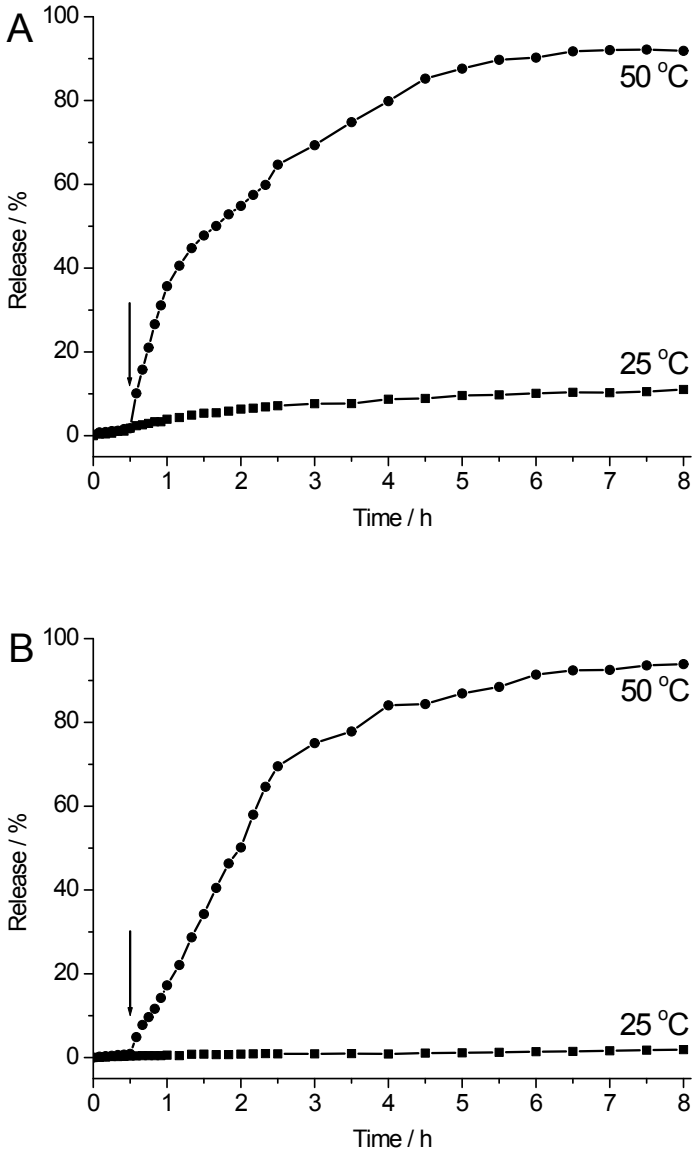

Fig. S23 Thermoresponsive simultaneous release profiles from spDNA-gated MSNs functionalized with Ti^{IV}-chelating phosphonates (MSN-PO-Ti-DNA) in Tris-HCl buffer (pH 7.4): (A) calcein (λ_{ex} = 458 nm, λ_{em} = 510 nm); (B) 9-aminoacridine (λ_{ex} = 400 nm, λ_{em} = 455 nm). The arrow indicates the change of temperature.

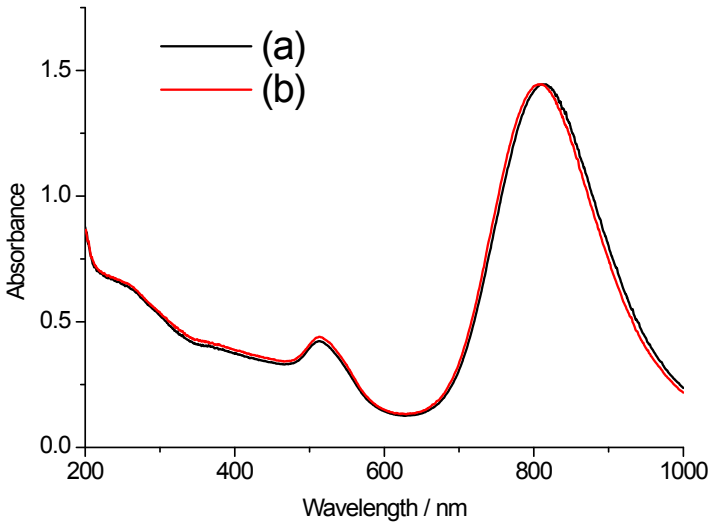

Fig. S24 UV-vis spectra of (a) GNRs and (b) GNR@MSNs.

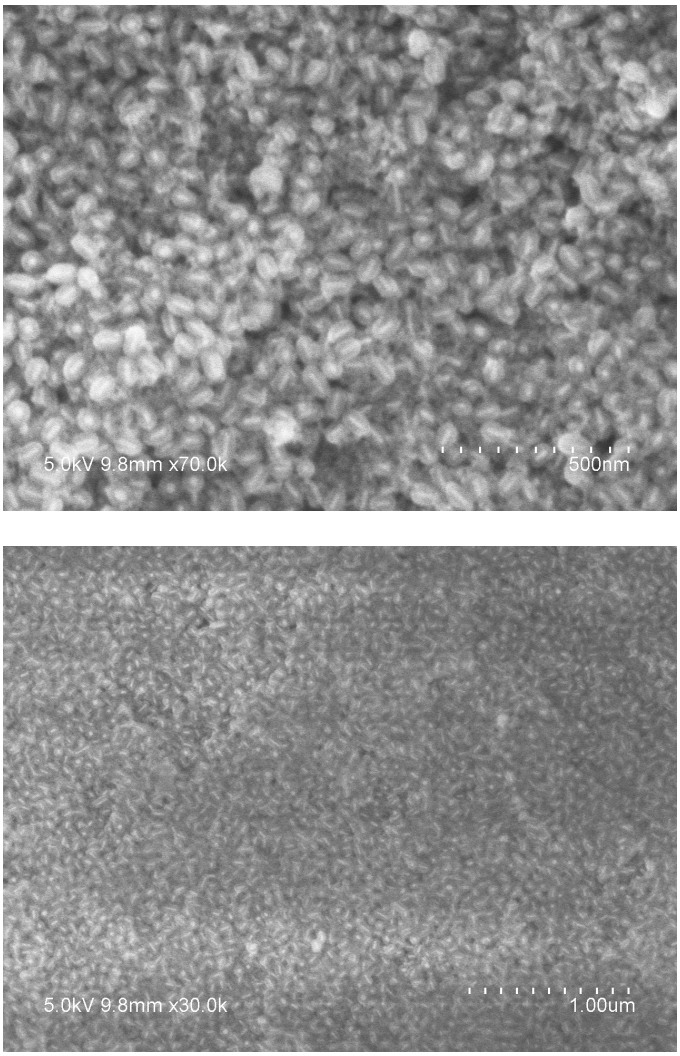

Fig. S25 SEM images of GNR@MSNs in different scales.

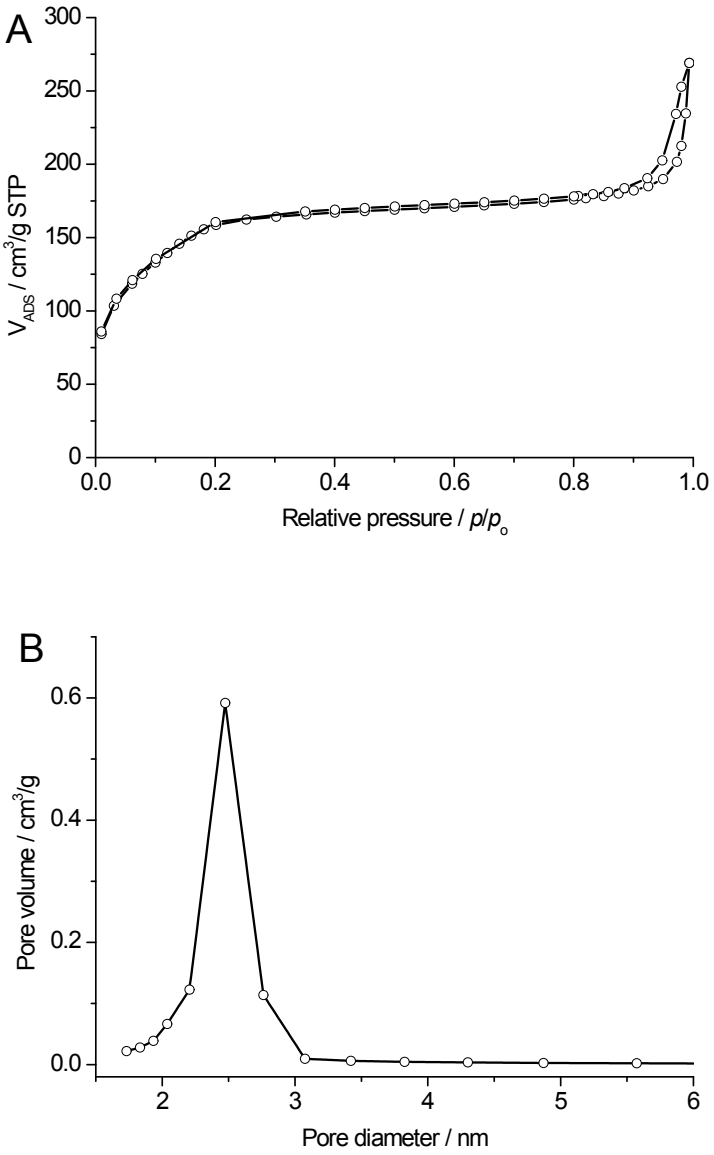

Fig. S26 (A) Nitrogen adsorption–desorption isotherms and (B) pore size distribution of GNR@MSNs.

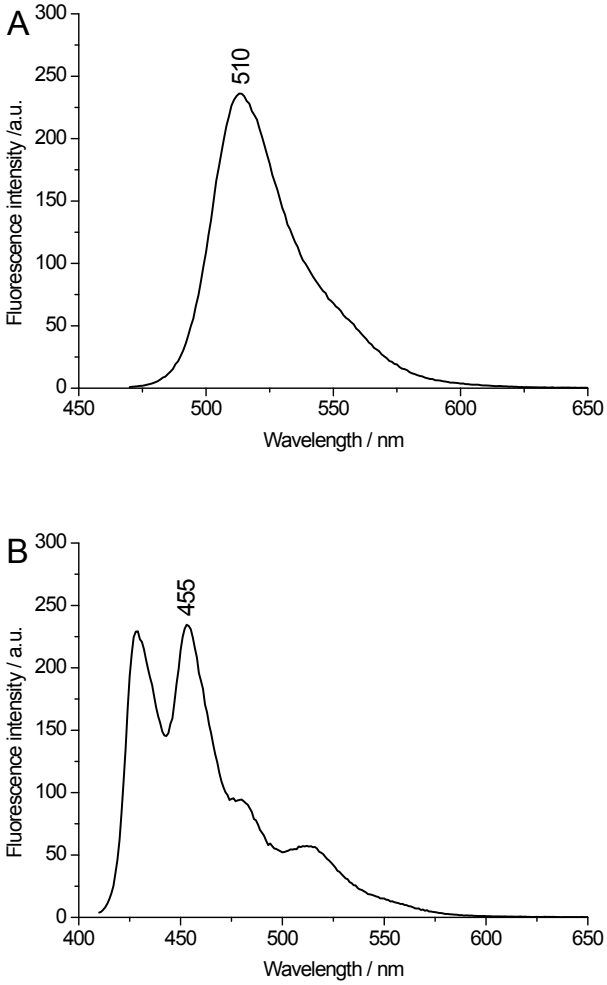

Fig. S27 Fluorescence spectra of final washing solutions containing (A) calcein and (B) 9-aminoacridine at the excitation wavelengths of 458 and 400 nm, respectively, in the case of spDNA-gated GNR@MSNs functionalized with phosphonate via Ti^{IV} coordination (GNR@MSN-PO-Ti-DNA).

The loading of calcein and 9-aminoacridine was carried out as follows. First, 4 mg of Ti^{IV}-chelating phosphonate-functionalized GNR@MSNs (GNR@MSN-PO-Ti) was suspended in 8 mL of aqueous calcein (0.4 mM) in PBS solution for calcein loading. Second, aqueous spDNA solution was added to the suspension for DNA capping. Third, 2 mL of aqueous 9-aminoacridine solution (1 mM) was added for 9-aminoacridine loading, followed by centrifugation and washing with PBS solution to remove excess dyes and DNA. Finally, the washing solutions were collected and diluted to a certain volume of 250 mL. The fluorescence spectra of the final washing solution were measured at different excitation wavelengths (Fig. S27), and the concentrations of calcein and 9-aminoacridine were determined from the standard curves of fluorescence intensity of aqueous calcein and 9-aminoacridine solution versus concentration (Fig. S5B and S6B), respectively. The differences between the initially added (total) and unloaded (washed) amounts of calcein and 9-aminoacridine were calculated to determine the loading capacities of calcein encapsulated within the Ti^{IV}-chelating phosphonate-functionalized GNR@MSNs (GNR@MSN-PO-Ti) and 9-aminoacrindine intercalating within the capped spDNA, respectively.

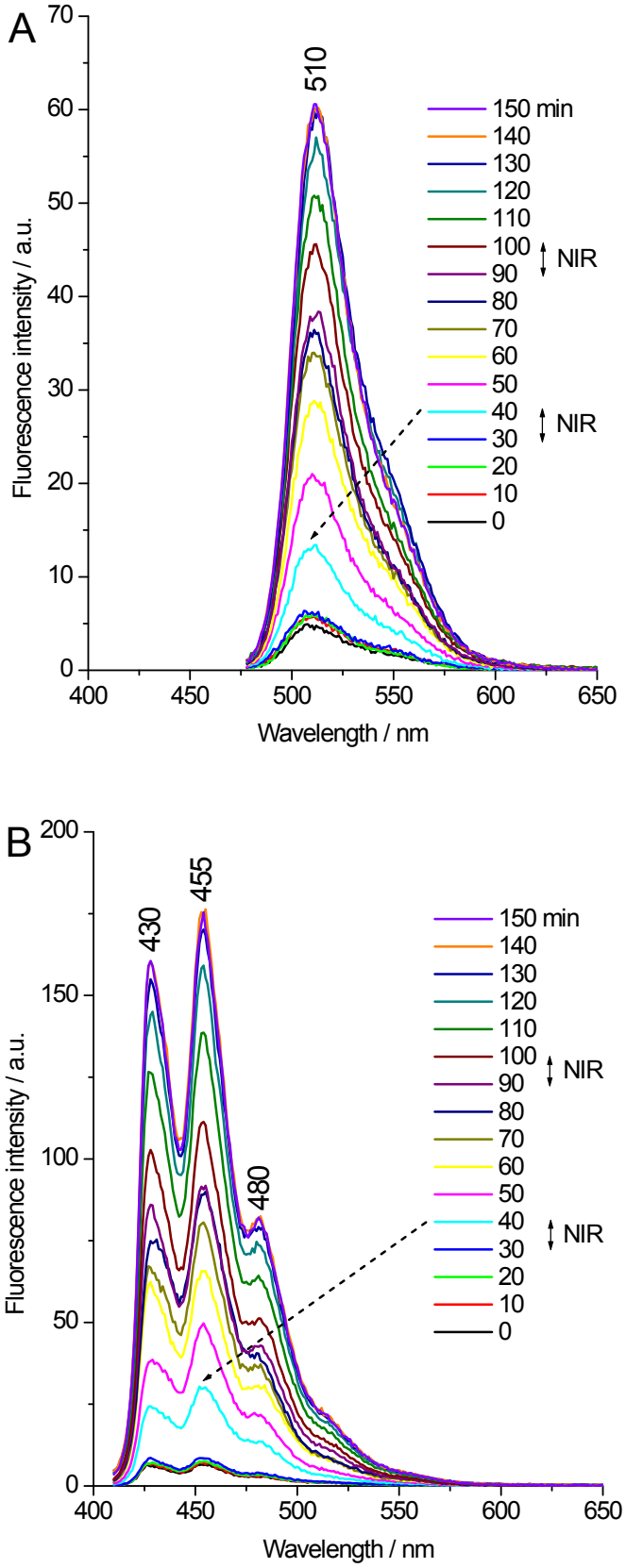

Fig. S28 Fluorescence spectra of dyes released from the PBS solution (pH 7.4) of GNR@MSN-PO-Ti-DNA upon irradiation of 808 nm NIR light at the power density of 3 W/cm^2 for 10 min interval: (A) calcein (λ_{ex} = 458 nm, λ_{em} = 510 nm); (B) 9-aminoacridine (λ_{ex} = 400 nm, λ_{em} = 455 nm).

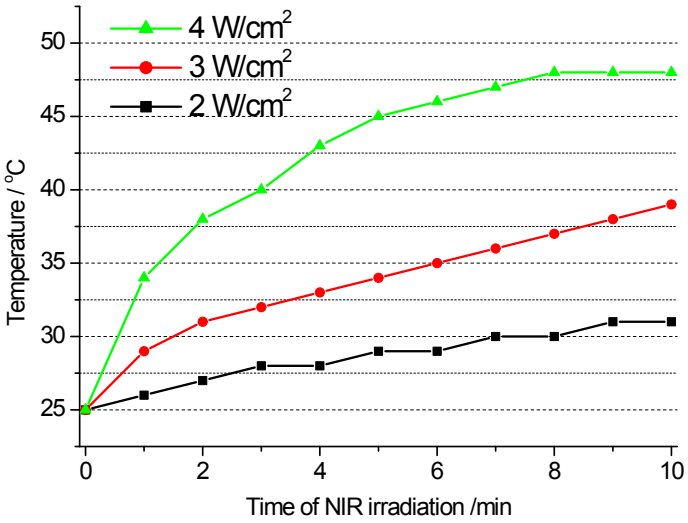

Fig. S29 Photothermal effects of GNR@MSNs (0.4 mg/mL) upon irradiation of 808 nm NIR light at different power densities for 10 min.

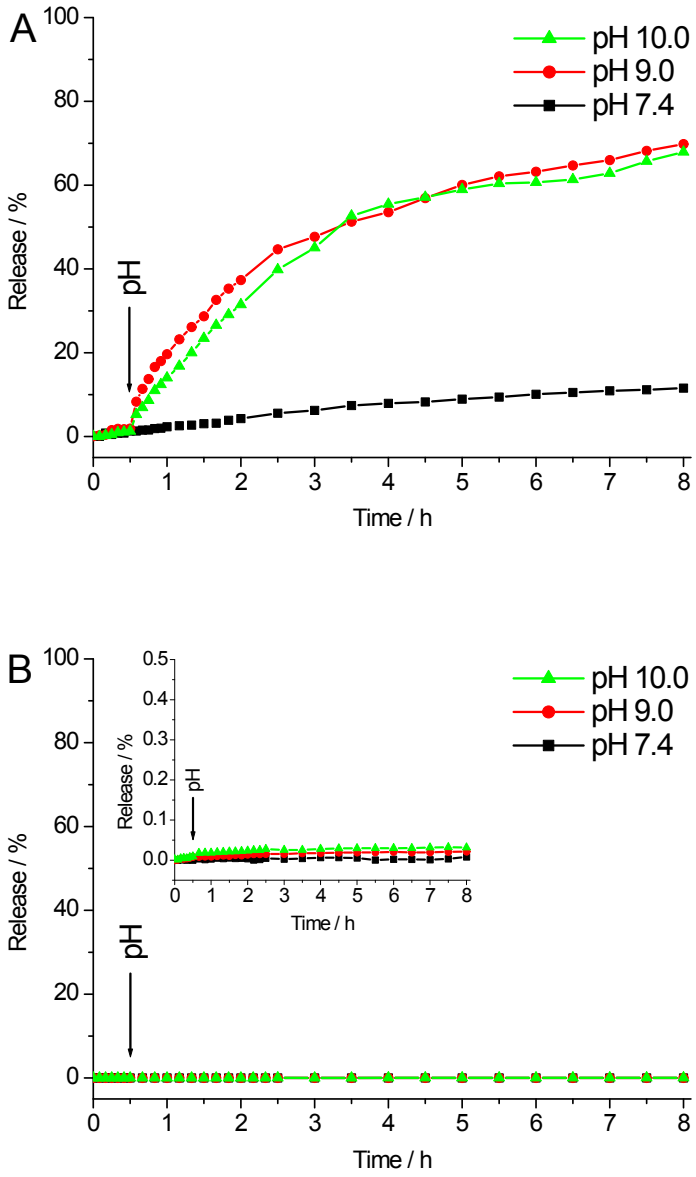

Fig. S30 pH-responsive release profiles of cargo from spDNA-gated MSNs functionalized with Ti^{IV}-chelating phosphonates (MSN-PO-Ti-DNA) in PBS solutions: (A) calcein (λ_{ex} = 458 nm, λ_{em} = 510 nm); (B) 9-aminoacridine (λ_{ex} = 400 nm, λ_{em} = 455 nm). Inset indicates the figure in a different scale. The arrow indicates the change of pH.

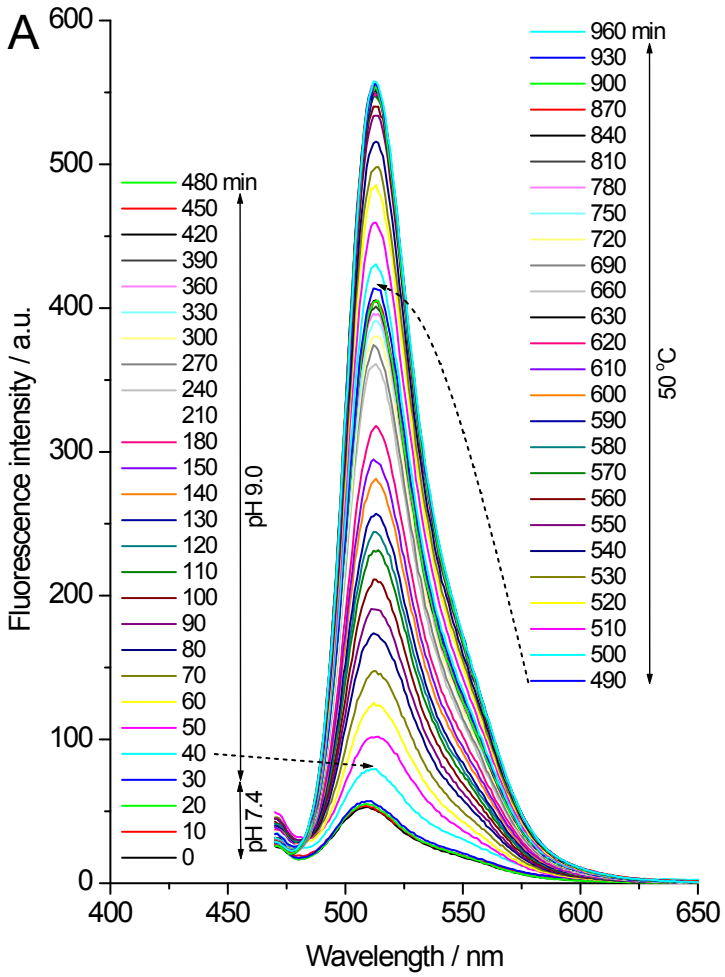

Fig. S31 Fluorescence spectra of dyes released from the PBS solution (pH 7.4) of spDNA-gated MSNs functionalized with Ti^{IV}-chelating phosphonates (MSN-PO-Ti-DNA) upon first trigger of pH 9.0 at 30 min and subsequent trigger of heating (50 °C) at 480 min: (A) calcein (λ_{ex} = 458 nm, λ_{em} = 510 nm); (B) 9-aminoacridine (λ_{ex} = 400 nm, λ_{em} = 455 nm).

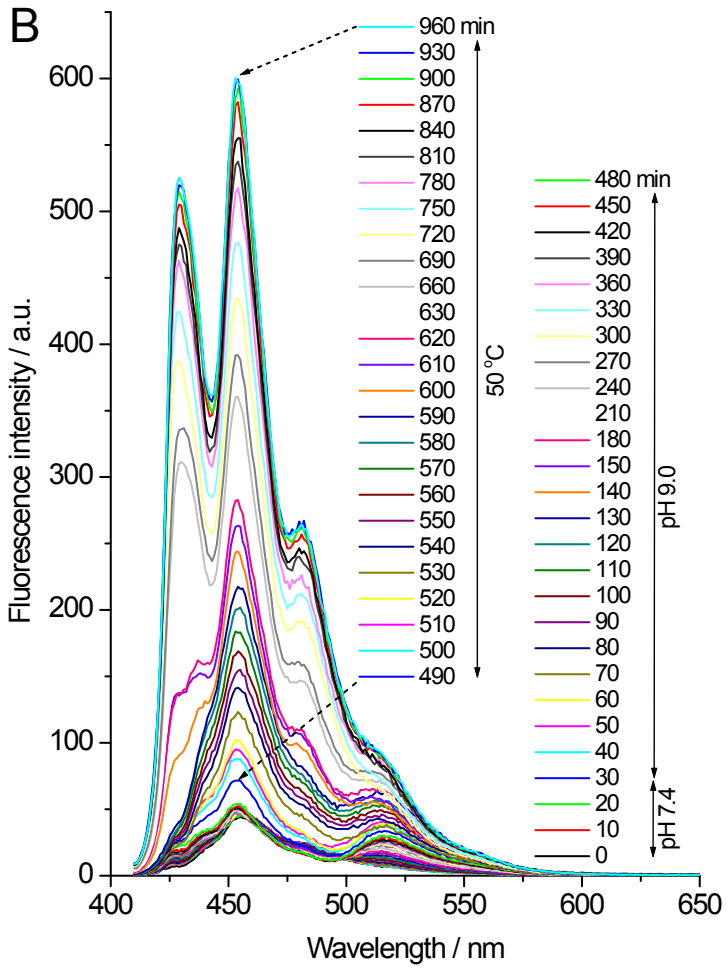

Fig. S31 (continuted)

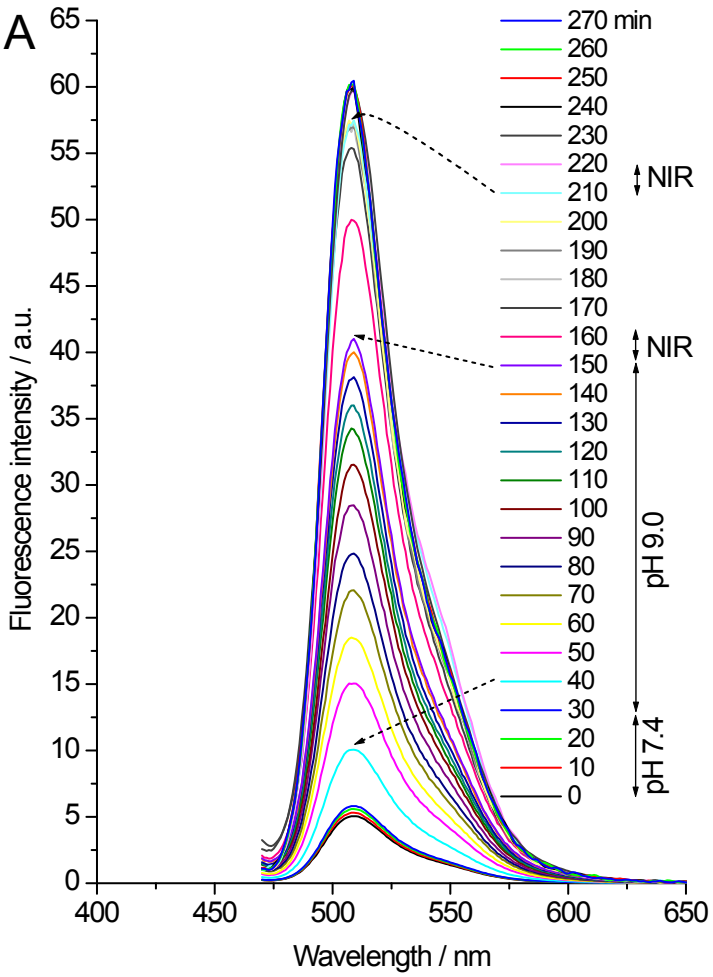

Fig. S32 Fluorescence spectra of dyes released from the PBS solution (pH 7.4) of spDNA-gated GNR@MSNs functionalized with Ti^{IV}-chelating phosphonates (GNR@MSN-PO-Ti-DNA) upon first trigger of pH 9.0 at 30 min and subsequent irradiation of 808 nm NIR light at the power density of 3 W/cm^2 for two 10-min intervals: (A) calcein (λ_{ex} = 458 nm, λ_{em} = 510 nm); (B) 9-aminoacridine (λ_{ex} = 400 nm, λ_{em} = 455 nm).

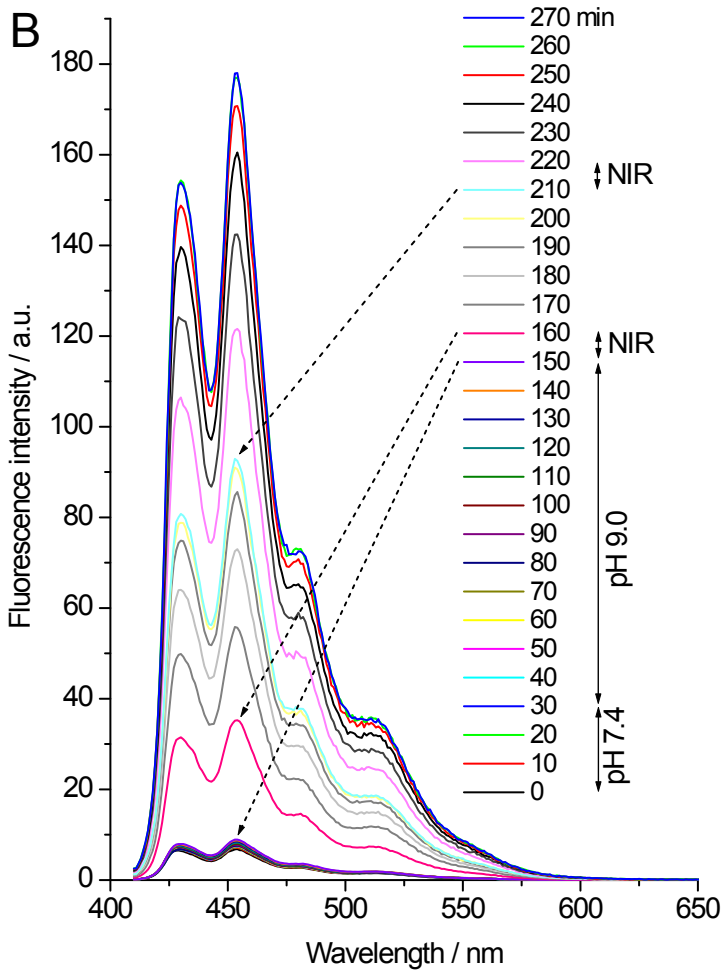

Fig. S32 (continuted)

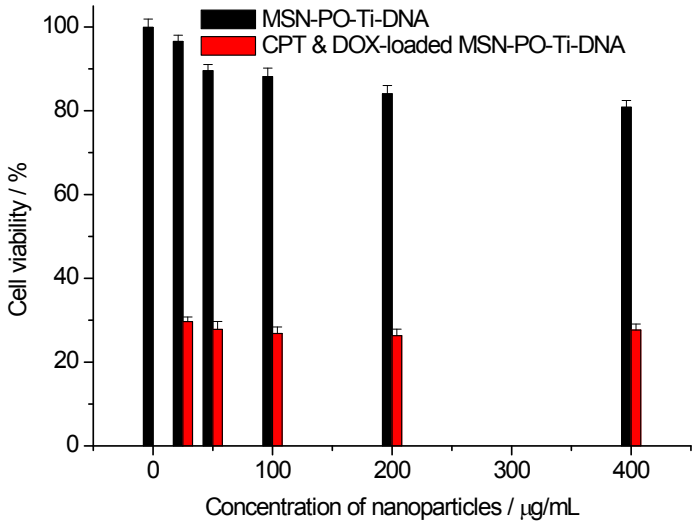

Fig. S33 In vitro cytotoxicity of spDNA-gated MSNs functionalized with Ti^{IV}-chelating phosphonates (MSN-PO-Ti-DNA) before and after loading of camptothecin (CPT) and doxorubicin (DOX) incubated with HepG2 cells for 24 h.

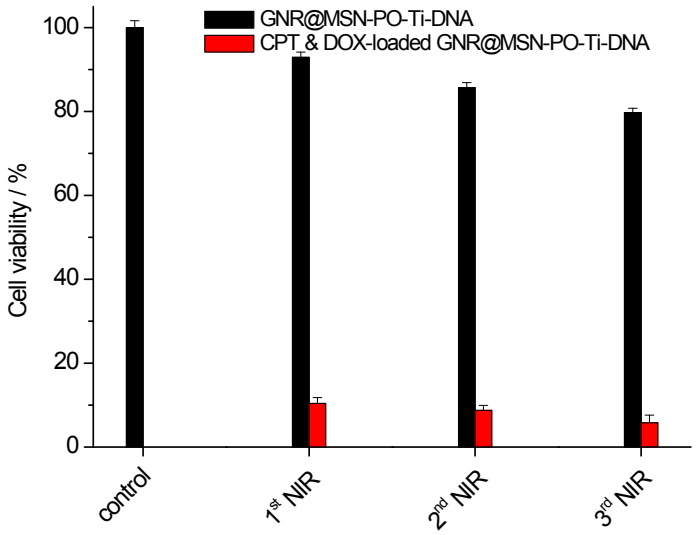

Fig. S34 In vitro cytotoxicity of spDNA-gated GNR@MSNs functionalized with Ti^{IV}-chelating phosphonates (MSN-PO-Ti-DNA) (20 μg/mL) before and after loading of CPT and DOX incubated with MCF-7 cells for 24 h followed by NIR irradiation using 808 nm light at the power density of 3 W/cm^2 in an ON (10 min)–OFF (50 min) sequence and another 24 h.

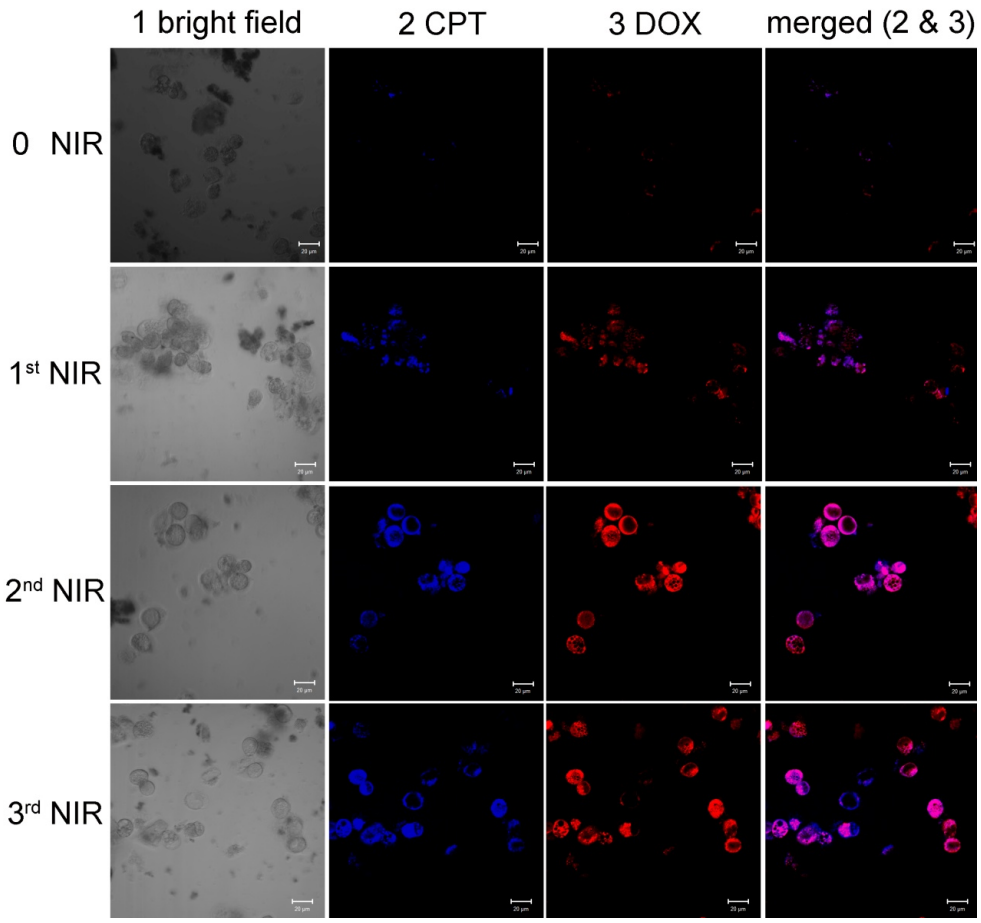

Fig. S35 CLSM images of cellular uptake of CPT- and DOX-loaded spDNA-gated GNR@MSNs functionalized with Ti^{IV}-chelating phosphonates (GNR@MSN-PO-Ti-DNA) (50 μg/mL) and their intracellular drug release behaviors after incubation with MCF-7 cells for 24 h before and after NIR irradiation of 808 nm light at the power density of 3 W/cm^2 in an ON (10 min)–OFF (50 min) sequence and 2 h incubation: CPT (λ_{ex} = 365 nm); DOX (λ_{ex} = 488 nm).